Starch-based double cross-linked amphoteric hydrogel: Synthesis, characterization and its dye adsorption study

Highlights

The current chapter describes the formation of a starch-based double cross-linked hydrogel containing both positive and negative charges. The amphoteric hydrogel was synthesized for the exclusion of anionic and cationic dyes from the waste aqueous solution. The formation of positive charge on the starch backbone occurs via the reaction of triethylamine with the open-up epoxy ring of epichlorohydrin, while the carboxylate ion of poly(acrylic acid) gives the negative charge in it. The amphoteric hydrogel was characterized by different spectroscopic and analytical techniques. Due to the formation of a double cross-linked network and the presence of quaternized alkyl chains, the hydrogel exhibits much lower swelling ability. As an adsorbent, the hydrogel was able to remove both cationic dye (methylene blue) and anionic dye (Congo red) with adsorption maxima of 133.65 mg/g and 64.73 mg/g, respectively. This study showed that the synthesized hydrogel offers remarkable performance as the toxic dye adsorbent for effluent treatment of wastewater.

Parts of this chapter are published as

[1] Sarmah, D. and Karak, N. Double network hydrophobic starch based amphoteric hydrogel as an effective adsorbent for both cationic and anionic dyes. *Carbohydrate Polymers*, 242:116320, 2020.

3.1. Introduction

The previous chapter (**Chapter 2**) described the preparation of a starch-acrylic acid (AA) hydrogel for agricultural applications. The hydrogel showed immense potential as a property enhancer for soil and has a controlled release ability of encapsulated materials. However, besides agricultural uses, hydrogels have huge applicability in wastewater treatment as discussed in **Chapter 1**. The adsorption ability of different charged or neutral species of the hydrogel matrix made them suitable for the removal of various pollutants from wastewater. Among these, dyes are one of the most toxic color-imparting agents used in various industries including paper, food, cosmetics, and more predominantly in textile industries [1-3]. The azo and aromatic groups of the dyes are responsible for the enormously growing environmental pollution due to their high toxicity and non-degradability nature. In addition to these, they are also carcinogenic as well as mutagenic due to the presence of carcinogenic derivatives such as naphthalene, benzidines, etc. [4-6]. Thus, the removal of these contaminates from wastewater has received utmost importance and hydrogels have been widely utilized for these purposes. Although water holding capacity is the main criterion of a hydrogel, but in some applications such as the removal of effluents from wastewater it will be more effective if the adsorbent can selectively adsorb the contaminants, not huge amounts of water. In addition to this, most of the literature reported hydrogels are selective adsorbents for either cationic or anionic dyes, only [7,8]. However, a few reports are available for the adsorption of both types of dyes, but adsorption efficiency was not satisfactory [9].

Hence, in the current work, we synthesized a starch-based hydrogel with amphoteric properties i.e., having both positive and negative charges on the network so that it can be able to adsorb both anionic and cationic dyes efficiently. Literature advocates the preparation of an amphoteric hydrogel for dye adsorption. For example, Shukla et al. synthesized an amphoteric hydrogel for the adsorption of both anionic dye (orange G) and cationic dye (methylene blue, MB). But the use of only synthetic monomers restricted its application [10]. Therefore, a new synthetic strategy was developed for the preparation of a bio-based amphoteric hydrogel in which starch was cross-linked with epichlorohydrin (ECH) with the subsequent addition of triethylamine (TEA) groups for the formation of positive charge. To incorporate the positive charge, TEA group reacts with the epoxy ring of ECH and the carboxylate ion of the *N, N*-methylene bis-acrylamide (MBA) cross-linked AA moiety provides the negative charge in it. The

incorporation of ECH as a cross-linker leads to high cross-linking density which reduces the hydrophilicity of the hydrogel, resulting in lower swelling ability. The hydrogel was utilized to remove the cationic dye MB and anionic dye Congo red (CR) from the waste aqueous solution. To evaluate the efficiency of the hydrogel different experimental conditions such as temperature, pH, dye concentration, ionic strength, etc. are altered to obtain the best result. The performance studies established that the synthesized amphoteric hydrogel is a proficient and sustainable dye adsorbent for wastewater purification.

3.2. Experimental

3.2.1. Materials

Various chemicals including tapioca starch, AA, ammonium per sulfate (APS), MBA, and sodium hydroxide (NaOH) were used as the same grade and specifications as discussed in **Chapter 2.**

ECH is a transparent liquid with molecular weight 92.52 g/mol and 1.18 g/cm^3 density. It was procured from SRL, India, and was used without further modification.

TEA is a colorless liquid with molecular weight 101.19 g/mol and density 0.726 g/cm^3 was purchased from Avantor, India.

CR is an azo dye containing a negatively charged group. It is a water-soluble compound with molecular weight 696.66 g/mol. It was brought from SDFCL, India.

MB is a thiazine dye with molecular weight 319.85 g/mol. It is a positive charge-containing dye and was purchased from LOBA Chemie, India.

3.2.2. Methods

3.2.2.1. Synthesis of the amphoteric hydrogel

The synthesis of the double cross-linked amphoteric hydrogel was done by a facile one-pot polymerization technique via a two-step reaction. The first step was performed in accordance with the method described previously by Stanciu et al. with minor modifications [11]. Briefly, 1 g of starch was stirred with 10 mL of water in a round bottom flask with a gradual increment of the temperature up to 60 °C. The mixture was stirred for 2 h for complete dispersion of starch as described in **Chapter 2**. Then an equimolar mixture of ECH and TEA was mixed under constant stirring for 30 min. After that, 3N aqueous NaOH solution was mixed dropwise and stirred for another 5 h at

60−70 °C. Viscosity was gradually increased after the formation of the ECH cross-linked quarternized starch. Subsequently, in the second step, the reaction chamber was deoxygenated by purging nitrogen gas and the temperature was gradually decreased so that the temperature of the reaction mixture became 50 °C. At that temperature, 0.683 g of AA diluted with water was mixed and stirred for another 15 min. Finally, aqueous solutions of cross-linker MBA (0.04 g) and initiator APS (0.01 g) were added with a gradual increase in temperature up to 70 °C, and polymerization was allowed to proceed. After stirring for 1 h the gel formation was completed, and the carboxylic group of the AA was neutralized with 8N aqueous NaOH solution. The gel was cut into pieces and used for swelling and dye adsorption study. Hydrogels with different cationic and anionic groups were prepared by varying ECH to TEA ratio and keeping the amount of AA constant as shown in **Table 3.1.** The three hydrogels with different compositions of ECH and TEA content were encoded as SETA1, SETA2, and SETA3. For comparison purposes, a hydrogel with only the first cross-linking network was prepared and encoded as SET.

Table 3.1. Different amounts of reactants used in the synthesis of the amphoteric hydrogels

Sample code	**Starch content (g)**	**ECH content (g)**	**TEA content (g)**	**MBA content (g)**	**APS content (g)**	**AA content (g)**
SETA1	1	0.240	0.263	0.010	0.04	0.683
SETA2	1	0.319	0.349	0.010	0.04	0.683
SETA3	1	0.398	0.433	0.010	0.04	0.683
SET	1	0.398	0.433	---	---	---

3.2.3. Structural analysis

FTIR spectra and XPS analysis were recorded by using the same instruments under the same conditions as mentioned in **Chapter 2** (Section **2.2.3**).

3.2.4. Swelling test

The swelling study of the synthesized SETAs was done using both the direct reaction product and dry hydrogel powder. A calculated amount of hydrogel samples was

immersed in distilled water. To determine the swelling ability similar method and mathematical equation were used as described **in Chapter 2.**

3.2.5. Dye adsorption study

To examine the dye adsorption ability, the calculated amount of the hydrogel was immersed in 100 mL of different dye solutions. When adsorption was proceeding, the samples were filtered, and 2 mL of dye solutions were extracted at a constant interval of time. The decreased dye concentration was determined by measuring absorbance at λ_{max} of each dye using a UV–vis spectrophotometer. The adsorption capacity at the equilibrium state was evaluated using the following equation.

Adsorption capacity, qe = {(Co−Ce)/M} × V ---------- Eq. 3.1

where qe (mg. g^{-1}) is the equilibrium dye adsorption capacity, Co is the initial, Ce is the final dye concentration (mg. mL^{-1}) in the solution, M (mg) is the weight of the hydrogel, and V (mL) is the volume of dye solution used [12].

Moreover, various conditions such as temperature, pH of the dye solution, the concentration of dye, ionic strength, etc. were varied and adsorption capacity was determined, as explained above. Moreover, the adsorption performance was also investigated in the MB/CR mixed system at different pH values (3, 6, 8, and 10). Although the λ_{max} of CR slightly shifted from 493 nm to 475 nm in the mixed system, but the decreased dye concentration of each dye in the mixed system was also measured at λ_{max} of individual dye.

3.2.5.1. Field emission scanning electron microscopy (FESEM) study after dye adsorption

FESEM was used to take the surface images of the SETA3 before and after dye adsorption by a Carl Zeiss Sigma VP equipment (accelerating voltage of 20 kV).

3.3. Results and discussion

3.3.1. Synthesis of the hydrogel

The synthetic route for the preparation of the double cross-linked amphoteric hydrogel is given in **Scheme 3.1**. The first step is the cross-linking of the primary hydroxyl group of starch via ring-opening polymerization of the epoxy group of ECH. In this step, some of

the epoxy rings quarternized through a reaction with TEA. While in the second step, AA is grafted with the remaining primary hydroxyl group of starch via free radical polymerization. In this step, MBA acts as a cross-linker to form the second network. ECH network is a tough and ductile network that helps in enhancing cross-link density of the hydrogel. The increase in cross-linking density decreases the swelling ability and this could be varied by changing the amount of ECH. In the last step, the introduction of AA generates hydrophilicity. The cationic group produced through quarterization of the epoxy group and the anionic group present in the AA moiety leads to the formation of an amphoteric hydrogel which helps in the adsorption of both anionic and cationic dyes effectively.

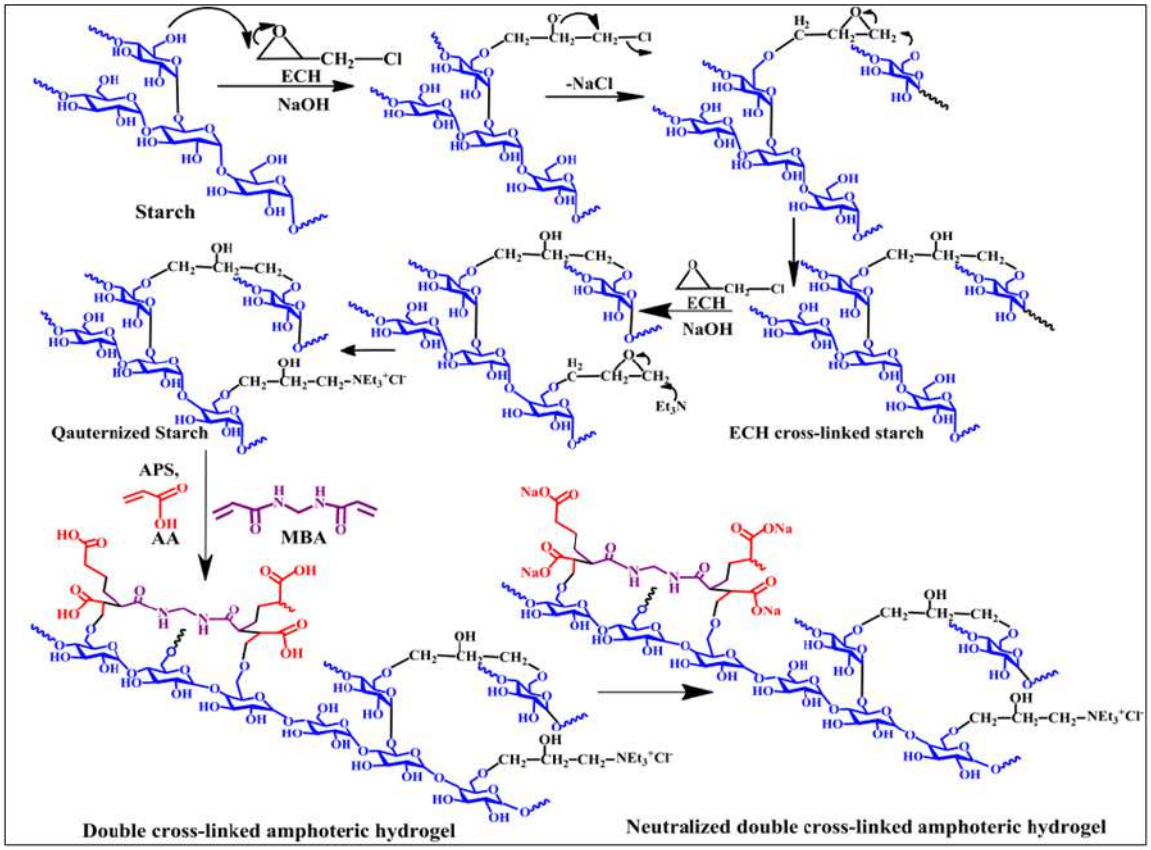

Scheme 3.1. Synthetic route of the double cross-linked amphoteric hydrogel.

3.3.2. Structural analysis

3.3.2.1. FTIR analysis

The structural conformation of the double cross-linked amphoteric hydrogel was performed by using FTIR spectroscopy. The FTIR spectra of bare starch, ECH, SET, and the hydrogels are shown in (**Figure 3.1.a** and **b**).

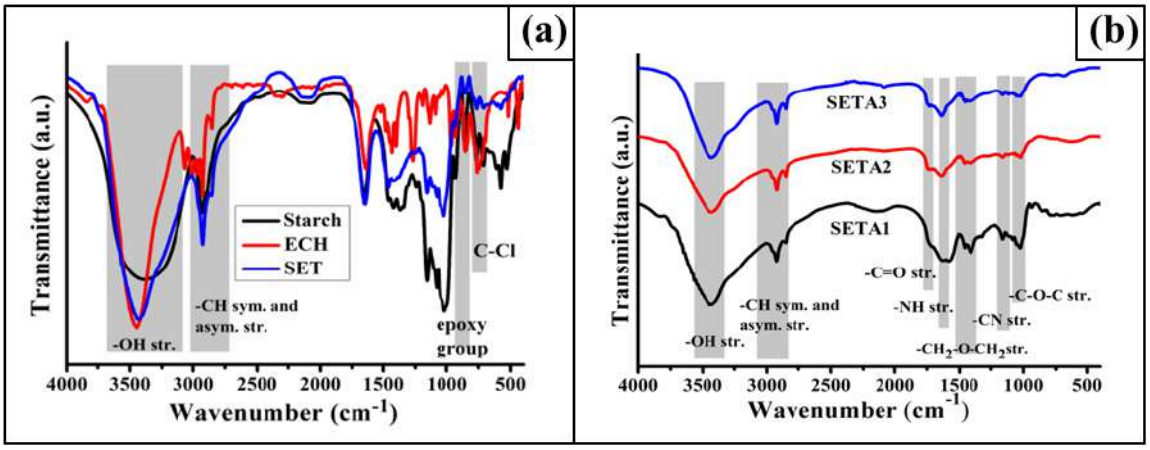

Figure 3.1. FTIR spectra of (a) ECH, starch, and SET (b) SETA1, SETA 2, and SETA3.

From the spectra, the intimate interactions between starch, ECH, TEA, and AA could be easily understood. The disappearance of characteristic peaks of ECH such as epoxy (853.88 cm^{-1}) and C-Cl (758.83 cm^{-1}) in the FTIR spectra of SET and the synthesized hydrogel indicates the opening of the epoxy ring [13]. Further, it also supports the cross-linking of ECH through the ether linkage with starch moiety. Moreover, the diminishing of the strength of the absorption bands of SET and the three SETAs at 3430.29 cm^{-1} indicates the decrease of hydrogen bonds and hydroxyl groups of starch; which confirms the cross-linking between starch and ECH [14,15]. In addition to this, the spectra also showed the characteristic bands for the successful grafting of AA on the starch backbone. The sharp band present at 2800–2922.60 cm^{-1} is attributed to the C-H symmetric and asymmetric stretching frequencies present in starch, AA, and ECH moieties. The band at 1726.92 cm^{-1} corresponds to the carboxylic group of AA as mentioned in **Chapter 2**. In addition, the bands at 1625.24 cm^{-1} represent –NH stretching frequency of the 2nd cross-linker, MBA. Moreover, the presence of a sharp band at 1399−1455 cm^{-1} represents the stretching vibration of $–H_2C–O–CH_2–$, which indicates the formation of ether linkage between AA and the primary hydroxyl group of the starch moiety [16]. This also supports the cross-linking between primary alcoholic groups of starch through ECH. Further, the band at 1162.98 cm^{-1} represents the –CN stretching frequency of TEA and MBA, which supports the quaternization of starch [17] and the presence of the cross-linker. Moreover, the characteristics band at 1021.63 cm^{-1} represents the –C–O–C– linkage of starch.

3.3.2.2. XPS analysis

The chemical composition of SETA3 was investigated by XPS studies (**Figure 3.2.a**).

The analysis showed that the hydrogel contains C, N, O, Na, and Cl with atomic fractions of 64.94%, 1.77 %, 28.96 %, 2.83%, and 1.55%, respectively. To understand the extent of the reaction, high-resolution XPS spectra of C 1s, O 1s, and N 1s were also analyzed (**Figure 3.2.b-d**).

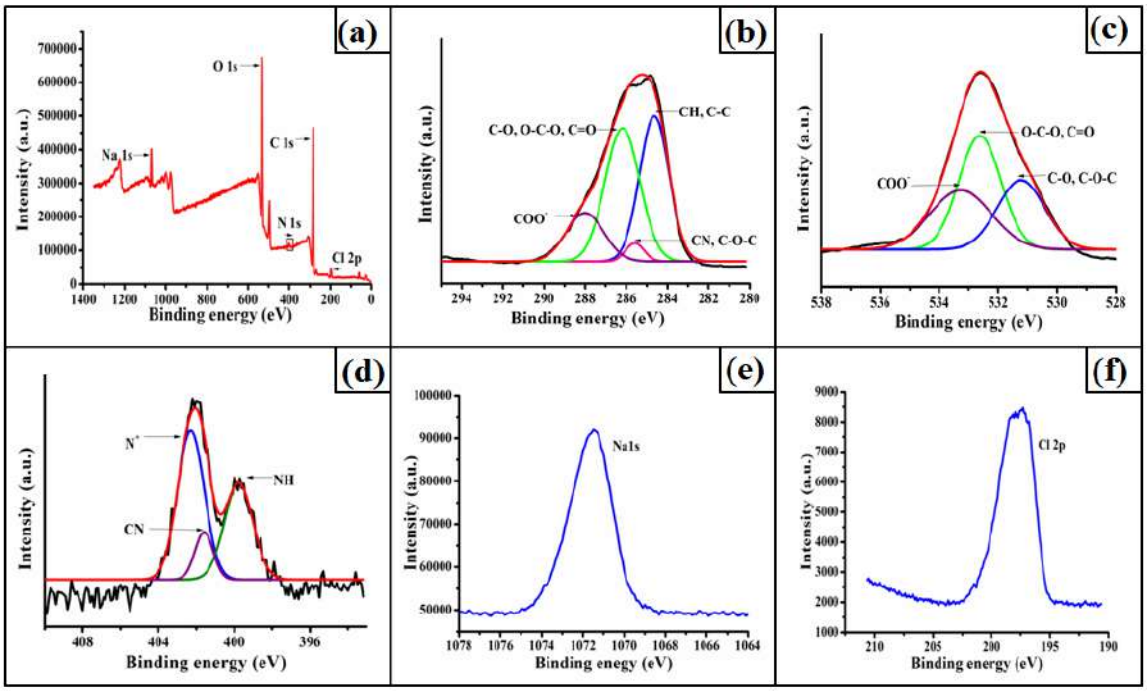

Figure 3.2. XPS spectra of (a) SETA3; (b) C 1s, (c) O 1s, (d) N 1s, (e) Na 1s, and (f) Cl 2p for SETA3.

The C 1s peak of SETA3 is deconvoluted into four peaks, which are assigned to C–H and C–C at 284.63 eV, C–N and C–O–C at 285.58 eV, O–C–O, C–O, and C=O at 286.18 eV and COO^- at 288.00 eV. All these are characteristic peaks for carbon-containing moieties starch, AA, MBA, ECH, and TEA. For O 1s, the peak at 531.22 eV is attributed to C–O, C–O–C groups, and the peaks at 532.61 eV and 533.27 eV are assigned to O–C–O and C=O, and COO^- groups, respectively [18]. These deconvoluted O 1s peaks confirmed the presence of AA moiety and the formation of ether linkage between starch and AA. Moreover, the N 1s spectrum is deconvoluted into three peaks at 399.76 eV, 401.59 eV, and 402.29 eV which are attributed to N–H, N–C, and N^+ groups, respectively [19]. These segments are due to the cross-linker MBA and TEA moiety of the hydrogel. Thus, from the high-resolution XPS study the presence of the quaternary ammonium group and COO^- group of AA in the hydrogel is confirmed. Thus, the XPS study established that the synthesized hydrogel was an amphoteric hydrogel having both positive and negative charges in it. Moreover, the XPS study also supports the presence

of Na and Cl in SETA3 (**Figure 3.2.e** and **f**). The Na atoms are coming from the NaOH that is used to neutralize the carboxylate groups of AA and the Cl atoms are due to the use of ECH.

3.3.3. Swelling of SETAs

The swelling values of all three hydrogels are shown in **Figure 3.3**.

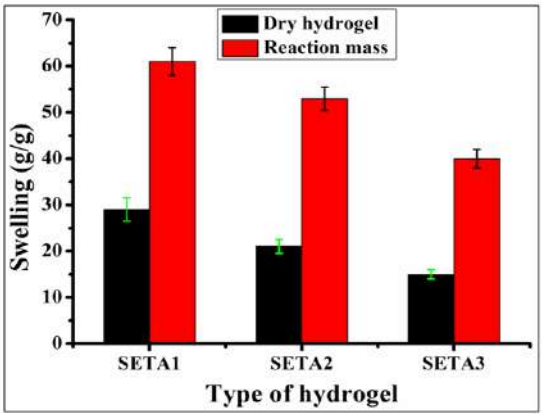

Figure 3.3. Swelling values of the hydrogels

It is seen that the synthesized hydrogel showed much lower water adsorption capacity although it contains hydrophilic PAA moiety compared to the conventional superabsorbent hydrogel. This observation demonstrated that internal hydrophobicity generates inside the hydrogel matrix which drastically decreases the swelling ability. This is due to the increased cross-linking density leading to a very compact structure by decreasing the distance between the cross-linked points. With an increase in the strength of the hydrogel, the pores between the cross-linked points lose their ability to open up too much. Hence, the pore size decreases resulting in lower swelling ability [16]. Moreover, the swelling ability also depends on the hydrophobic functional groups present in the three-dimensional network of the hydrogel. The formation of long alkyl on the starch backbone through quaternization using TEA also provides hydrophobicity to the hydrogel. The hydrophobicity increased with the increase in the amount of TEA to ECH ratio [11]. Moreover, the dry hydrogel showed much lower swelling than the direct gel, obtained as the reaction product. This is due to the reason that upon drying at elevated temperature the cross-linking of the hydrogel increased too much and hence the pore volume decreased, resulting in low water absorption.

3.3.4. Dye adsorption

To evaluate the performance of the synthesized hydrogel as an adsorbent, a liquid-phase dye adsorption analysis was carried out. As the hydrogel contained both cationic and anionic groups in its network, it can be able to combine with the anionic and cationic groups of dye molecules through electrostatic interactions. Here, cationic dye, MB, and anionic dye CR were chosen for the study. SETA3 can be able to adsorb the water contaminant (dye) efficiently with a limited amount of water owing to the lowest swelling ability. Hence, all the adsorption performance was carried out using SETA3 as the representative hydrogel. It is well known that the removal efficiency of soluble dyes is dependent on the solution temperature, pH, salt concentration, equilibrium adsorption time, initial concentration of dye, etc. The influence of these parameters on dye adsorption was studied comprehensively to obtain the best adsorption result.

3.3.4.1. Effect of adsorbent dosages

Figure 3.4. (**a** and **b**) displays the effect of hydrogel dose on the removal percentage of MB and CR. The color removal efficiency enhanced with an increase in adsorbent dosages and reached up to 98.41% with 45 mg adsorbent dosages for MB and 95.64% for 80 mg adsorbent dosages in the case of CR. This phenomenon can be attributed due to the presence of a greater charge functional group which enhanced the availability of the active adsorbent sites with an increase in adsorbent dosages. **Figure 3.4.**(**c** and **d**) displays the effect of adsorbent dosages on the adsorbent amount. It is seen that, although the adsorption percentages increase from 94.5% to 98.41% and 91.46% to 95.64% in the case of MB and CR, respectively, but adsorption amount (qe) decreases. Hence, with a combination of adsorption efficiency and adsorption amount (qe) the optimized dosages for MB and CR are 35 mg and 70 mg, respectively. Moreover, with these optimized adsorbent dosages the adsorption capacity of the synthesized hydrogels: SETA1, SETA2, and SETA3 was evaluated for both dyes (**Figure 3.4.e**). As expected, the dye adsorption capacity for CR increased with the increase of ECH to TEA ratio due to the more positive charge in the polymer matrix. Hence, SETA3 owned the highest adsorption capability (64.73 mg/g) for CR, while the adsorption declined gradually in the case of SETA2 and SETA1. However, the adsorption capability for MB was found to be higher in the case of SETA1 than SETA2 and SETA3. But the capacity was not differed too much for the other two hydrogels, due to the presence of the almost same amount of anionic groups (COO^-) in the hydrogel networks for all the cases.

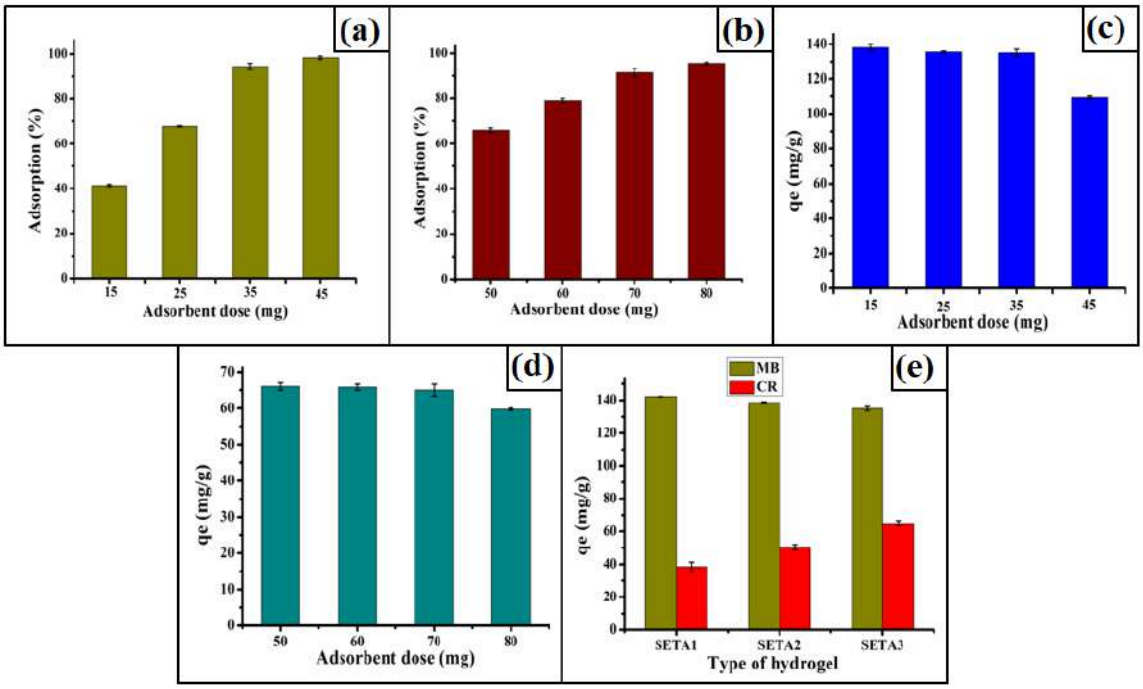

Figure 3.4. (a) Effect of adsorbent dosages on adsorption of MB, (b) effect of adsorbent dosages on adsorption of CR, (c) effect of adsorbent dosages on adsorption amount for MB, and (d) effect of adsorbent dosages on adsorption amount for CR; (e) dye adsorption capacity of the three SETAs, (dye concentration 50 ppm, 100 mL; temperature 323 K, pH: 8 for MB and 6 for CR).

3.3.4.2. Effect of initial dye concentration

The effect of initial dye concentration (from 10 ppm to 50 ppm) on the adsorption performance of the hydrogel was also investigated keeping the optimized amount of the adsorbent. It is clearly seen from the figure that with the increase in concentration of dye from 10 ppm to 50 ppm, the adsorption amount was enhanced (**Figure 3.5. a**). However, the corresponding adsorption efficiency declined from 99.5% to 92.6% in the case of MB and 95.1% to 90.26% for CR (**Figure 3.5.b**). This may be explained on the basis of the fact that at a lower dye concentration (10 ppm) due to the availability of sufficient numbers of active adsorption sites, a higher percentage of adsorption was observed. In contrast, with the increase in dye concentration, there is a lower percentage of availability of the active adsorption sites of the hydrogel surface [20,21]. As a result, a lower percentage of adsorption has been monitored at higher dye concentrations.

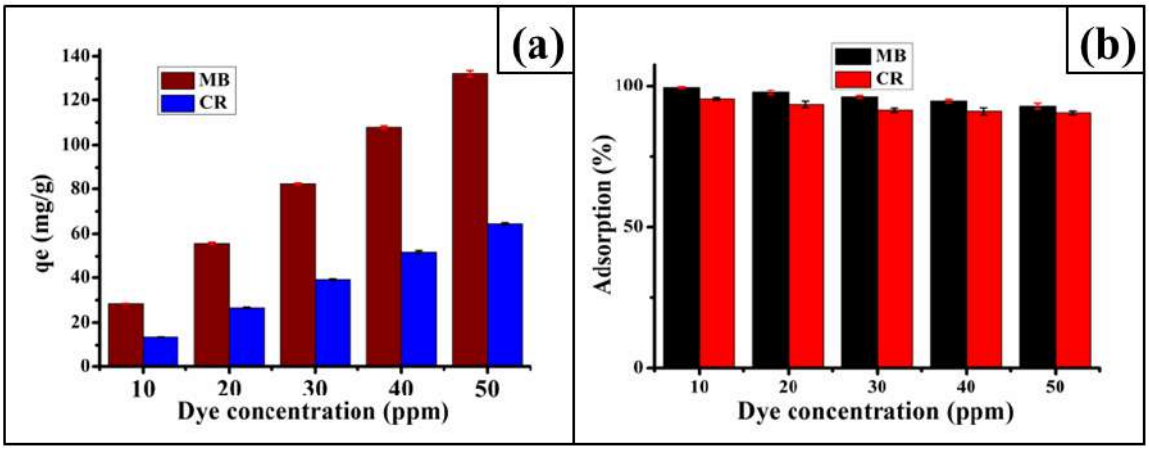

Figure 3.5. (a) Effect of dye concentration on adsorption amount, and (b) effect of dye concentration on adsorption, and (dye concentration 50 ppm, 100 mL; adsorbent dosage: 35 mg for MB and 70 mg for CR, temperature 323 K, pH: 8 for MB and 6 for CR).

3.3.4.3. Effect of temperature

Figure 3.6.a shows the effect of temperature on dye adsorption capacity. With the rise in temperature from room temperature (RT) to 323 K the adsorption efficiency for both MB and CR was enhanced. With the rise in temperature from room temperature (RT) adsorption efficiency for the dye molecules increased. This is due to the reason that the penetration of the dye molecules from the solution depends on their interactions with the polymer network. At RT, all the dye molecules are unable to penetrate the adsorbent matrix. With the increase in temperature, more numbers of dye molecules acquire enough energy to undergo interaction with the active sites of adsorbent surfaces [22]. In addition, with the increase in temperature, the swelling of the hydrogel may also enable the passage of a huge number of dye molecules resulting in a higher rate of adsorption. Further, the increasing temperature lowers the solution viscosity which enhanced the diffusion rate of the dye molecules toward the adsorbent matrix resulting in a higher rate of adsorption. This proves the endothermic nature of the adsorption process.

3.3.4.4. Effect of pH

Figure 3.6.b demonstrates the effect of pH on the adsorption performance of the synthesized amphoteric hydrogel. During the experiment, in the case of MB, the pH of the aqueous solutions varied from 3 to 10. CR is a diazo dye and the initial pH affects its molecular form in an aqueous solution [23]. At lower pH its color changes from red to dark blue, therefore in this section, the pH of CR solution was varied from 6 to 10. The

medium pH affects the adsorption capacity of the hydrogel. In the case of MB at pH 3, much lower adsorption was observed. In an acidic environment, the excess of H^+ ions in the aqueous solution competes with the positively charged dye molecules to interact with the carboxylate ion resulting lowering of adsorption [7]. However, under the alkaline condition (pH 8) a higher adsorption percentage for MB was observed due to an increase in the electrostatic attraction forces. This phenomenon is due the increment of the negative active sites, due to the deprotonation of the carboxylic groups of the AA chain. However, further, increase in pH from 8 the electrostatic attraction between MB and COO^- was partially destroyed due to the charge screening effect of the excess Na^+ ions [24]. In contrast, the highest adsorption for CR was at pH 6 and further decreased with increasing pH. The number of negative charge increases with the increase in pH of the system and compete with the negatively charged dye to get attached to the active site of the adsorbent through electrostatic interactions. This leads to a lower percentage of adsorption.

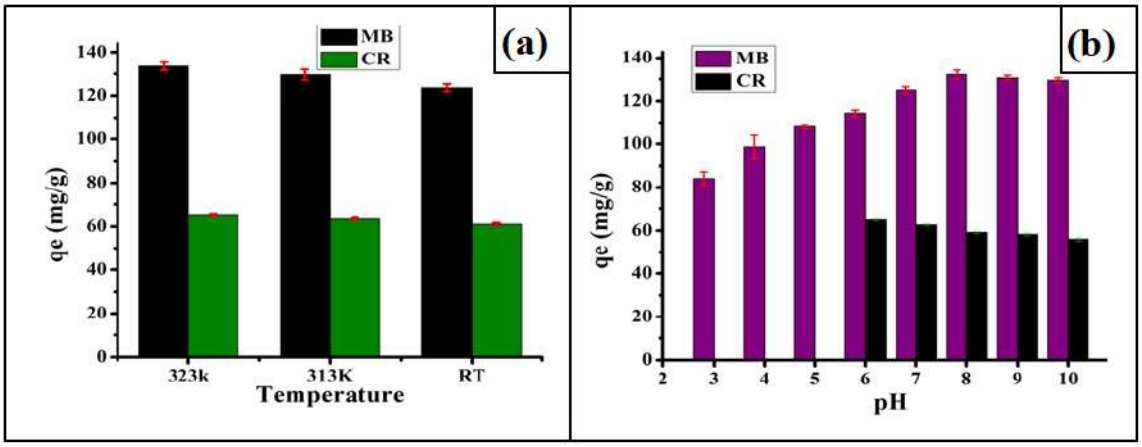

Figure 3.6. (a) Effect of temperature on adsorption, and (b) effect of pH on adsorption, (dye concentration 50 ppm, 100 mL; adsorbent dosage: 35 mg for MB and 70 mg for CR, temperature 323 K, pH: 8 for MB and 6 for CR).

3.3.4.5. Effect of contact time

Figure 3.7.(**a** and **b**) shows the effect of time on the dye removal efficiency of the hydrogel. The equilibrium adsorption time for MB and CR was found to be 100 min and 75 min, respectively. After this particular time, the dye adsorption was leveled off. The rate of adsorption is higher at the initial stage compared to the equilibrium time. This observation indicates that at first there may be some electrostatic interactions of the charged active site of the hydrogel with the dye molecules. After this interaction, there

may be mass transfer through swelling of the hydrogel which leads to hydrogen bonding or van der Waals interactions. The decreased intensity of the UV–vis spectra of both the dyes with time are shown in **Figure 3.7.c** and **d.**

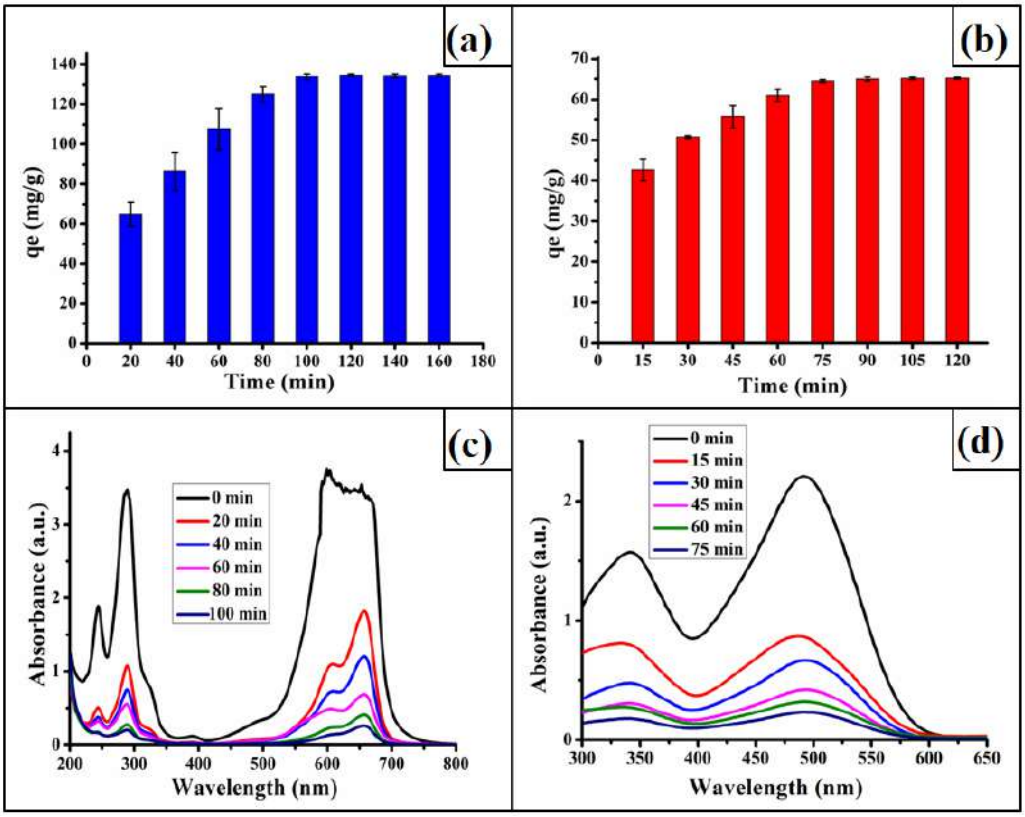

Figure. 3.7. (a) Effect of contact time on adsorption of MB, (b) effect of contact time on adsorption of CR, (c) UV–vis spectra of adsorbed MB solution with time, and (d) UV–vis spectra of adsorbed CR with time, (dye concentration 50 ppm, 100 mL; adsorbent dosage: 35 mg for MB and 70 mg for CR, temperature 323 K, pH: 8 for MB and 6 for CR).

3.3.4.6. Kinetics of adsorption

Adsorption kinetics is a vital tool to predict the adsorption phenomenon and the rate of adsorption. Further, the contact time to reach equilibrium is a significant factor for dye adsorption in real applications. During adsorption, adsorbate molecules migrate from the solution to the adsorbent's outer surface, followed by diffusion into the boundary layer, and finally the complete mass transfer takes place via internal pore diffusion. Thus, to figure out the adsorption mechanism pseudo-first-order model, pseudo-second-order model, and intra-particle diffusion model were investigated. The linear form of first, second-order [25], and intra-particle diffusion kinetics [24] are represented in **Eq.(3.2)–**

(3.4), respectively.

$$\log(q_e - q_t) = -k_1/2.303t + \log q_e \text{ ---------- Eq.3.2}$$

$$t/q_t = 1/q_e t + 1/k_2 q_e^2 \text{ ---------- Eq.3.4}$$

$$q_t = k_3 t^{1/2} + C \text{ ---------- Eq.3.4}$$

where qe is the equilibrium adsorption capacity and qt (mg/g) is the adsorption at time t (min); k_1 (min^{-1}), k_2 (g. $mg^{-1}.min^{-1}$) and k_3 ($mg/g.min^{-1/2}$) describe the rate constants of the pseudo-first-order model, pseudo-second-order model, and intra-particle diffusion model, respectively and C is the boundary layer thickness. Linear plots for log (qe-qt) against t and (t/qt) against t for pseudo-first and second-order models and qt against $t^{1/2}$ for the intra-particle model are shown in **Figure 3.8.(a–c)**. The closeness of the linear correlation coefficient (R^2) to unity is a good agreement with the pseudo-second-order models. However, the linear correlation coefficients in the case of the pseudo-first-order model for MB and CR were found to be 0.9016 and 0.8277, respectively. The correlation coefficient value indicates that the pseudo-second-order model is more reliable which suggested that chemisorption occurs via ionic interaction between the adsorbate and adsorbent, and it is the rate-determining step [26]. The results obtained from the different kinetics models are depicted in **Table 3.2**.

The kinetics data were also analyzed by using the intra-particle diffusion model. According to this model, the greater the intercept (C) larger the boundary layer thickness. Moreover, if this process involved in the adsorption process; the plot qt versus $t^{1/2}$ should be a straight line and if it plays a major role in the rate-determining step of adsorption the straight line should pass through the origin [27]. However, if it exhibits multilinear plots, then more than one process simultaneously operates during adsorption. From **Figure 3.8.c,** it is seen that there are two linear regions for the plots, qt versus $t^{1/2}$. This result indicates that two or more processes affect the adsorption of CR and MB on the hydrogel. The linear region of the plot is associated with the diffusion of the adsorbate through the aqueous solution to the boundary layer of the hydrogel. The second phase is the internal diffusion towards the adsorbent's interior part. Moreover, none of the plots passing through the origin indicate that not only intra-particle diffusion took place, but also other mechanisms must associate with the adsorption process [28,29]. The presence of intercepts in the plots indicates the boundary layer thickness which also proves this fact. Thus, it can be suggested that along with surface adsorption intraparticle diffusion took place concurrently.

From the kinetics study, it can be concluded that the dye adsorption process takes place in a three-step mechanistic route. In the first step, the dye molecules are transported from the bulk solution to the outer surface of the hydrogel. The second step is the penetration of the adsorbent to the interior part of the hydrogel and the third step is the adsorption of the charged adsorbate onto the oppositely charged active sites in the inner and outer portions of the adsorbent [28,29].

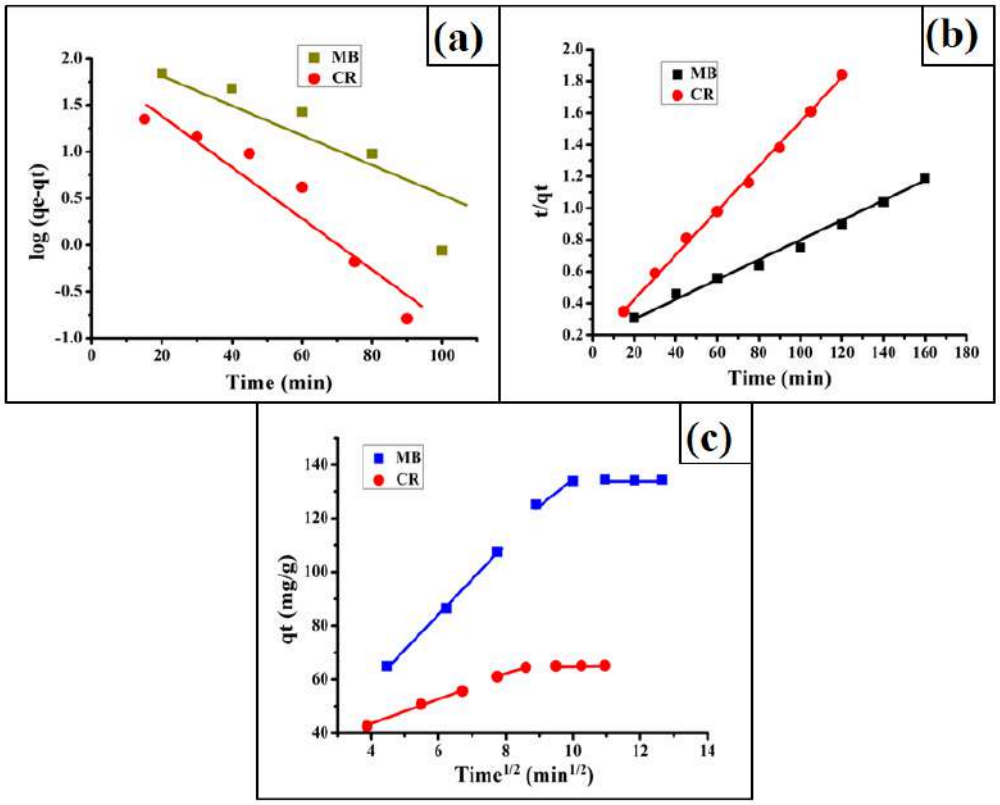

Figure 3.8. (a) Pseudo-first-order kinetics for MB and CR, (b) pseudo-second-order kinetics for MB and CR, (c) intra-particle diffusion models for MB and CR, (dye concentration 50 ppm, 100 mL; adsorbent dosage: 35 mg for MB and 70 mg for CR, temperature 323 K, pH: 8 for MB and 6 for CR).

Table 3.2. The kinetics parameters for adsorption of MB and CR on SETA3

Model	Kinetic parameters	MB	CR
Pseudo-first-order	k_1	5.1×10^{-2}	6.4×10^{-2}
Pseudo-second-order	K_2	1.37×10^{-2}	3.1×10^{-2}
	R^2	0.9902	0.9976
Intra-particle diffusion	K_3	8.9	3.29
	C	34.19	32.73

3.3.4.7. Isotherm study

The adsorption isotherm explains the interactions between the adsorbent and the adsorbate molecules. Langmuir and Freundlich adsorption isotherms are used to analyzed the dye adsorption mechanism **Figure 3.9.**(**a** and **b**). The mathematical expressions for Langmuir and Freundlich adsorption isotherms are represented as-

$$\mathbf{Ce/qe = 1/qmCe + K_L/qm} \quad \text{---------- Eq.3.5}$$

$$\mathbf{lnqe = lnK_F + 1/n\ lnCe} \quad \text{---------- Eq.3.6}$$

where Ce ($mg.L^{-1}$) is the dye concentration in equilibrium, qe (mg. g^{-1}) is the equilibrium adsorbed amount, qm (mg. g^{-1}) denotes the utmost adsorption capacity, K_L and K_F (L. mg^{-1}) are the Langmuir and Freundlich constants. The Langmuir constant K_L (L. mg^{-1}) relates to the affinity and free energy towards adsorption, while the slope of the Freundlich isotherm represents the intensity of adsorption [25]. The results obtained from the intercept and slopes of the linear plots for Langmuir (Ce/qe against Ce) and Freundlich (lnqe against lnCe) isotherms are tabulated in **Table 3.3**. The data was found to disagree with the Langmuir model with a very poor correlation factor, which assumes that multilayer adsorption takes place during the dye uptake. However, the data are best fitted with the Freundlich adsorption isotherm with a high correlation factor for both dyes. The result reveals that multilayer adsorption occurs on heterogeneous surfaces in accordance with the Freundlich adsorption isotherm. The slope (1/n) of the Freundlich adsorption isotherm indicates the favorability of the adsorption process. If the 1/n value is between 0.1 and 1, then the adsorption process is admiring, while a lower value of 1/n than 1 represents the adsorption involved in the chemical process [3]. The 1/n values for both MB and CR in between 0.1 and 1 indicate that chemisorption is the preferred adsorption process. These results also support the electrostatic attraction of the dye on the active sites of the adsorbent.

Table 3.3. The isotherms parameters for adsorption of MB and CR on SETA3

Model	Isotherm parameters	MB	CR
Langmuir Isotherm	q_m	149.25	125
	K_L	0.67	4.87
	R^2	0.9427	0.9125

Freundlich Isotherm	n	2.80	1.48
	K_F	78.26	21.48
	R^2	0.9859	0.9963

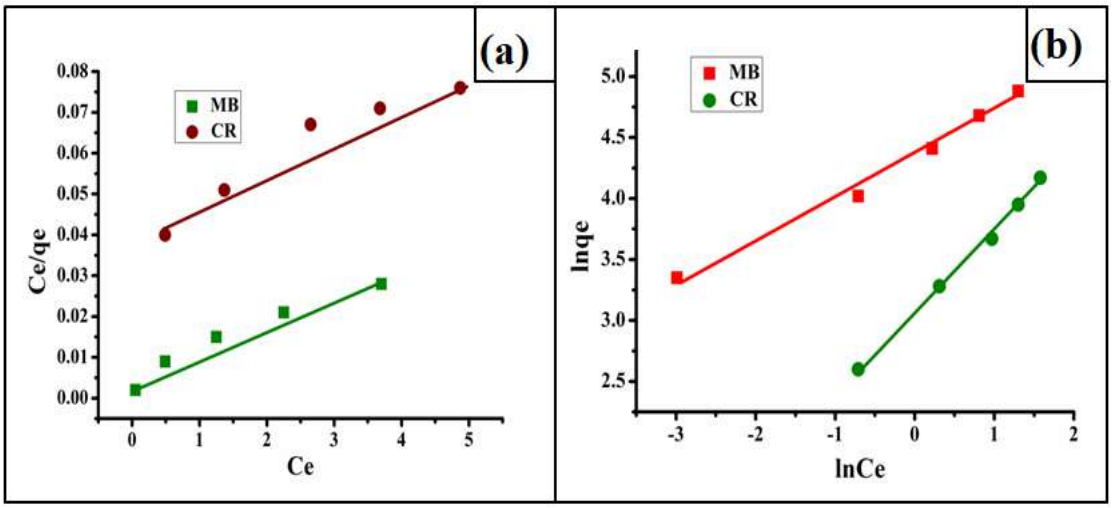

Figure. 3.9. (a) Langmuir adsorption isotherm for MB and CR, and (b) Freundlich adsorption isotherm (dye concentration 50 ppm, 100 mL; adsorbent dosage: 35 mg for MB and 70 mg for CR, temperature 323 K, pH: 8 for MB and 6 for CR).

3.3.4.8. Dye adsorption in a mixed system

To investigate the usefulness of SETA3 the dye adsorption experiment was also done in a mixed system (**Figure 3.10)**. It was found that compared to single system, the dye adsorption capacity enhanced in the mixed system. It is noted that the λ_{max} of each dye was decreased at the mixer. This may be due to the reason that, all the charged groups can be effectively used for the adsorption of both positive and negatively charged dye molecules simultaneously. Hence, electrostatic interactions occurred in all charged groups of the hydrogel effectively. To investigate selective adsorption, the dye adsorption experiment was also carried out in different pH values, at pH 3 and 6 (acidic) and pH 8 and 10 (basic). It was shown that at acidic pH (3 and 6) the adsorption percentage for CR is 98.64% and 97.34%, respectively. While at that pH, the adsorption performance for MB was 77.62% and 95.94%, respectively. On the other hand at pH 8 and 10, the adsorption percentage for MB was 99.9% and 98.48% and for CR 95.58% and 87.92% respectively. The decreased UV–vis spectra of the dye mixer and their photos at different pH values are shown in **Figure 3.10.b**.

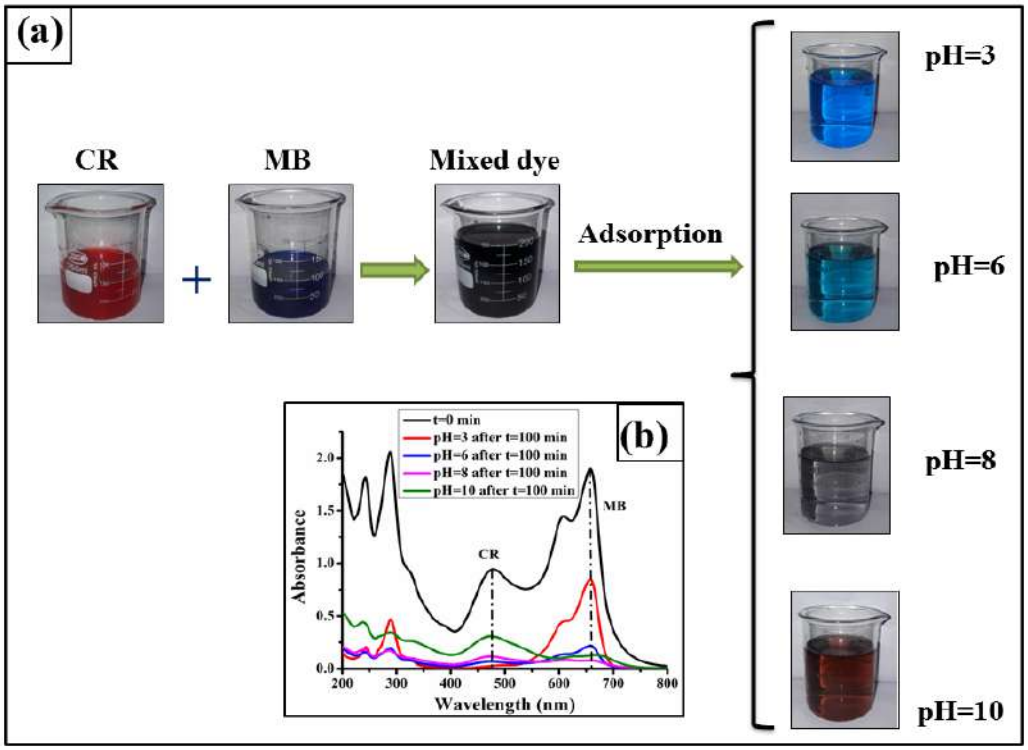

Figure 3.10. (a) Digital photos and (b) UV–vis spectra of MB/CR mixture before and after adsorption at different pH values (dye concentration 50 ppm for each dye, 200 mL; adsorbent dosage: 50 mg, temperature 323 K)

3.3.4.9. Dye adsorption mechanism

Various factors including interaction between adsorbent and adsorbate, their physical and chemical structures, and mass transfer process influence the dye adsorption mechanism. When the hydrogels are allowed to swell in a dye solution, then the dye molecules migrate onto the hydrogel surface and are adsorbed through van der Waals interactions and hydrogen bonding [30] Subsequently, electrostatic interactions occurred between the charged groups on the hydrogel with the cationic and anionic groups of dyes (**Scheme 3.2.**). A higher amount of total content in cationic (–N ($C_2H_5^+$)) or anionic ($–COO^-$) groups can provide a higher number of sites for the dye binding, thus can enhance the dye adsorption capacity of the hydrogel.

(a) FTIR analysis

FTIR spectral analysis was done on dye-adsorbed SETA3 and shown in Figure **3.11.a.** After adsorption, the adsorbent shows some characteristic peaks that confirm the conjugation of MB, CR, and mixer of these two. With the addition to the characteristic peaks of SETA3, an evident peak at 1570 cm^{-1} in the FTIR spectrum of CR adsorbed

SETA3 and mix dye adsorbed SETA3 is assigned to the –N=N– group of CR [31]. Moreover, in the FTIR spectra of MB-adsorbed SETA3 and mix dye-adsorbed SETA3, there is an evident peak in 1580 cm^{-1} which is due to the aromatic ring of MB [32]. Thus, FTIR analysis supports the adsorption of dye molecules on SETA3.

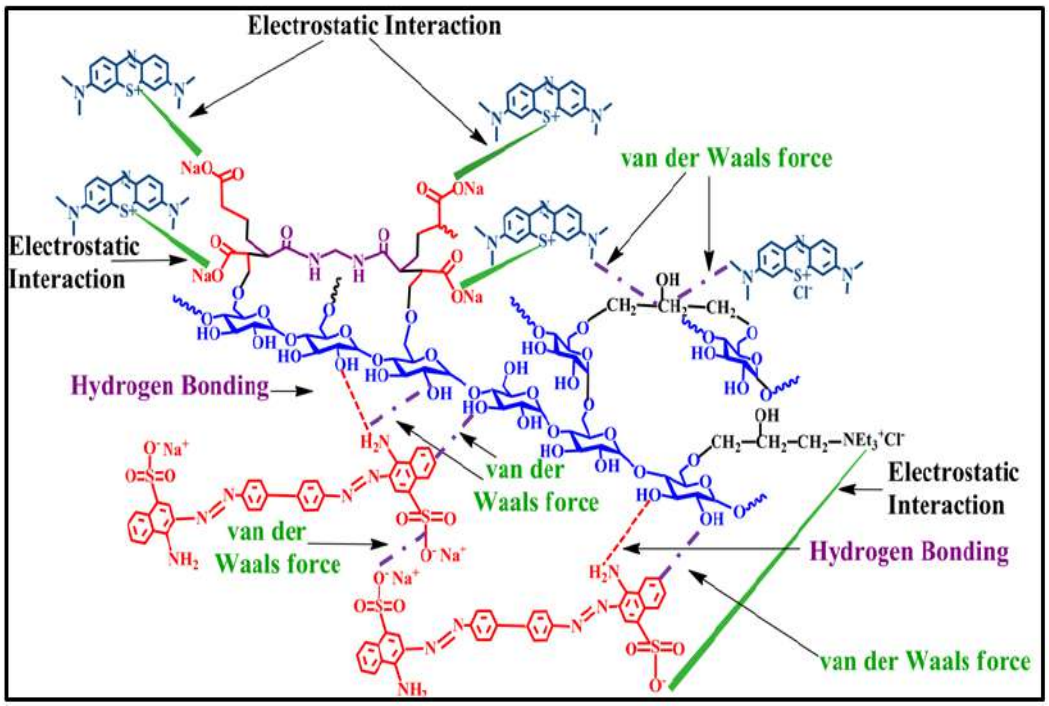

Scheme 3.2. Schematic representation for the possible interactions between the hydrogel and dye molecules.

(b) FESEM analysis

To investigate the surface morphology of SETA3 before and after adsorption FESEM analysis was also performed. **Figure 3.11.b** represents the FESEM images of the SETA3 before the adsorption of the dye molecule. It is seen that the surface of SETA3 is completely smooth without any roughness. Figure (**3.11.c** and **d**) represents the FESEM images of the synthesized hydrogels after adsorption of MB and CR, respectively. It is clearly seen that the surface of SETA3 exhibited a totally different morphology after absorption of the dye molecules. The surface of SETA3 becomes uneven and rougher due to the presence of the dye molecules. Moreover, it is also seen that both MB and CR adsorbed SETA3 exhibited a completely different surface morphology. MB adsorbed SETA3 exhibited a surface full of interconnected clouds like rough particles. In contrast, the CR adsorbed SETA3 contains the comparatively greater size of different irregular shapes like pentagons, hexagons, squares, triangles, and various other shapes also. Figure

3.11.(**e** and **f**) represents the surface morphology of SETA3 after adsorption of MB and CR mixer at two different magnifications.

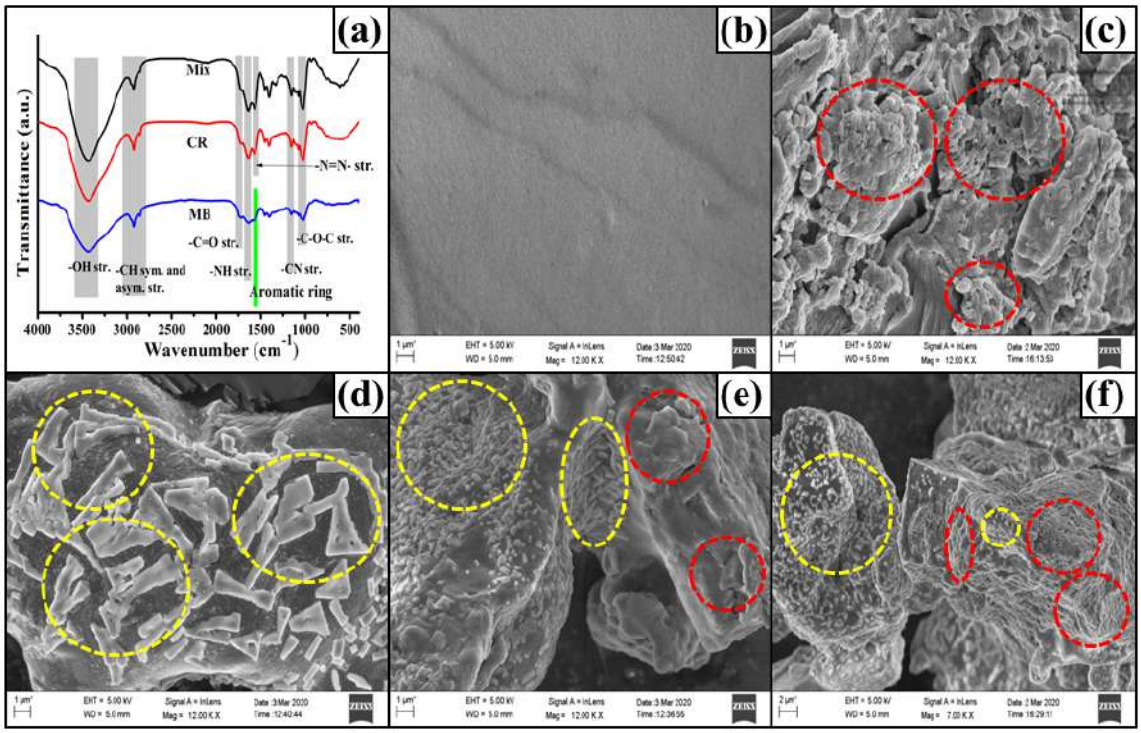

Figure 3.11. (a) FTIR spectra of MB, CR, and mixed dye adsorbed SETA3; FESEM images of (b) SETA3, (c) MB adsorbed SETA3, (d) CR adsorbed SETA3, and (e, f) mix dye adsorbed SETA3.

The mixed dye adsorbed SETA3 exhibited an interrelated surface morphology with both of the dye molecules as seen from these figures. This phenomenon proves the collaborative effect of both of the adsorbed dye molecules, which can be attributed due to the electrostatic contact between the charged groups of the adsorbate. The similarity of the mixed dye adsorbed surface with the individual dye adsorbed surface was also reported by various kinds of literature such as Liu et al. [33]. Some parts of the surface similarity of mix-dye adsorbed SETA3 with the individual dye adsorbed SETA3 are shown with red and yellow dotted lines.

3.4. Conclusion

In conclusion, the work has introduced a facile method to obtain a new kind of starch-based amphoteric hydrogel having both cationic (Et_3N^+) and anionic (COO^-) groups. Three hydrogels with different compositions were successfully synthesized via a two-step one-pot procedure. The hydrogel shows remarkable potential in wastewater

purification with the potential to adsorb both anionic and cationic dyes simultaneously with high efficiency. From the kinetics study, it can be concluded that the adsorption process follows a three-step route which is obeying pseudo-second-order kinetics. Further, Freundlich isotherm was the best-fitted adsorption isotherm with a high correlation factor. In conclusion, the synthesized hydrogel can give a noteworthy contribution to hydrogel research. We also expect that this work would lead to the improvement of advanced water purification techniques.

References

[1] Pearce, C. I., Lloyd, J. R., and Guthrie, J. T. The removal of colour from textile wastewater using whole bacterial cells: a review. *Dyes and Pigments*, 58(3):179-196, 2003.

[2] Shi, Y., Xue, Z., Wang, X., Wang, L., and Wang, A. Removal of methylene blue from aqueous solution by sorption on lignocellulose-g-poly (acrylic acid)/montmorillonite three-dimensional cross-linked polymeric network hydrogels. *Polymer Bulletin*, 70(4):1163-1179, 2013.

[3] Bello, K., Sarojini, B. K., Narayana, B., Rao, A., and Byrappa, K. A study on adsorption behavior of newly synthesized banana pseudo-stem derived superabsorbent hydrogels for cationic and anionic dye removal from effluents. *Carbohydrate Polymers*, 181:605–615, 2018.

[4] Güven, O., Şen, M., Karadağ, E., and Saraydın, D. A review on the radiation synthesis of copolymeric hydrogels for adsorption and separation purposes. *Radiation Physics and Chemistry*, 56(4):381-386, 1999.

[5] Thakur, S., Pandey, S., and Arotiba, O. A. Development of a sodium alginate-based organic/inorganic superabsorbent composite hydrogel for adsorption of methylene blue. *Carbohydrate Polymers*, 153:34-46, 2016.

[6] Mahmoud, G. A., Abdel-Aal, S. E., Badway, N. A., Elbayaa, A. A., and Ahmed, D. F. A novel hydrogel based on agricultural waste for removal of hazardous dyes from aqueous solution and reuse process in a secondary adsorption. *Polymer Bulletin*, 74(2):337-358, 2017.

[7] Crini, G., Peindy, H. N., Gimbert, F., and Robert, C. Removal of CI Basic Green 4 (Malachite Green) from aqueous solutions by adsorption using cyclodextrin-based adsorbent: Kinetic and equilibrium studies. *Separation and Purification Technology*, 53(1):97-110, 2007.

[8] Mahdavinia, G. R., Aghaie, H., Sheykhloie, H., Vardini, M. T., and Etemadi, H. Synthesis of CarAlg/MMt nanocomposite hydrogels and adsorption of cationic crystal violet. *Carbohydrate Polymers*, 98(1):358-365, 2013.

[9] Cui, W., Ji, J., Cai, Y. F., Li, H., and Ran, R. Robust, anti-fatigue, and self-healing graphene oxide/hydrophobically associated composite hydrogels and their use as recyclable adsorbents for dye wastewater treatment. *Journal of Materials Chemistry A*, 3(33):17445-17458, 2015.

[10] Shukla, N. B., Rattan, S., and Madras, G. Swelling and dye-adsorption characteristics of an amphoteric superabsorbent polymer. *Industrial & Engineering Chemistry Research*, 51(46):14941-14948, 2012.

[11] Stanciu, M. C., and Nichifor, M. Influence of dextran hydrogel characteristics on adsorption capacity for anionic dyes. *Carbohydrate Polymers*, 199:75–83, 2018.

[12] Lu, J., Li, Y. Y., and Zhou, Y. B. Adsorption properties of modified straw materials for dye and heavy metals removal in high salt wastewater. *Acta Scientiae Circumstantiae*, 38(10):3395–3401, 2019.

[13] Song, Y., Li, L., and Zheng, Q. Influence of epichlorohydrin modification on structure and properties of wheat gliadin films. *Journal of Agricultural and Food Chemistry*, 57(6):2295–2301, 2009

[14] Chen, X., Zhou, S., Zhang, L., You, T., and Xu, F. Adsorption of heavy metals by graphneoxide/cellulose hydrogel prepared from NaOH/urea aqueous solution. *Materials*, 9(7):582, 2016

[15] Zhang, L., Zhou, J., and Zhang, L. Structure and properties of β-cyclodextrin/cellulose hydrogels prepared in NaOH/urea aqueous solution. *Carbohydrate Polymers*, 94(1):386–393, 2013.

[16] Sarmah, D. and Karak, N. Biodegradable superabsorbent hydrogel for water holding in soil and controlled-release fertilizer. *Journal of Applied Polymer Science*, 137(13):48495, 2020.

[17] Qi, X., Li, Z., Shen, L., Qin, T., Qian, Y., Zhao, S., and Shen, J. Highly efficient dye decontamination via microbial salecan polysaccharide-based gels. *Carbohydrate Polymers*, 219:1-11, 2019.

[18] Zhang, M., Song, L., Jiang, H., Li, S., Shao, Y., Yang, J., and Li, J. Biomass based hydrogel as an adsorbent for the fast removal of heavy metal ions from aqueous solutions. *Journal of Materials Chemistry A*, *5*(7):3434-3446, 2017.

[19] Li, D., Li, Q., Bai, N., Dong, H., and Mao, D. One-step synthesis of cationic hydrogel for efficient dye adsorption and its second use for emulsified oil separation. *ACS Sustainable Chemistry & Engineering*, 5(6):5598–5607, 2017.

[20] Mahmoodi, N. M. Equilibrium, kinetics, and thermodynamics of dye removal using alginate in binary systems. *Journal of Chemical and Engineering Data*, 56(6):2802–2811, 2011.

[21] Yu, H. R., Hu, J. Q., Liu, Z., Ju, X. J., Xie, R., Wang, W., and Chu, L. Y. Ion-recognizable hydrogels for efficient removal of cesium ions from aqueous environment. *Journal of Hazardous Materials*, 323:632-640, 2017.

[22] Ghorai, S., Sarkar, A. K., Panda, A. B., and Pal, S. Effective removal of Congo red dyefrom aqueous solution using modified xanthan gum/silica hybrid nanocomposite as adsorbent. *Bioresource Technology*, 144:485-491, 2013.

[23] Lian, L., Guo, L., and Guo, C. Adsorption of Congo red from aqueous solutions onto Ca-bentonite. *Journal of Hazardous Materials*, 161(1):126–131, 2009.

[24] Qin, T., Qian, Y., Zhao, S., and Shen, J. Highly efficient dye decontamination via microbial salecan polysaccharide-based gels. *Carbohydrate Polymers*, 219:1-11, 2019.

[25] Zhou, L., Huang, J., He, B., Zhang, F., and Li, H. Peach gum for efficient removal of methylene blue and methyl violet dyes from aqueous solution. *Carbohydrate Polymers*, 101:574–581, 2014.

[26] d'Halluin, M., Rull-Barrull, J., Bretel, G., Labrugère, C., Le Grognec, E., and Felpin, F. X. Chemically modified cellulose filter paper for heavy metal remediation in water. *ACS Sustainable Chemistry & Engineering*, 5(2):1965–1973, 2017.

[27] Uğurlu, M. Adsorption of a textile dye onto activated sepiolite. *Microporous and Mesoporous Materials*, 119(1-3):276–283, 2009.

[28] Ai, L., Li, M., and Li, L. Adsorption of methylene blue from aqueous solution with activated carbon/cobalt ferrite/alginate composite beads: Kinetics, isotherms, and thermodynamics. *Journal of Chemical and Engineering Data*, 56(8):3475–3483, 2011.

[29] Ai, L., Zhang, C., and Meng, L. Adsorption of methyl orange from aqueous solution on hydrothermal synthesized Mg–Al layered double hydroxide. *Journal of Chemical and Engineering Data*, 56(11):4217–4225, 2011.

[30] Gong, R., Ye, J., Dai, W., Yan, X., Hu, J., Hu, X., and Huang, H. Adsorptive removal of methyl orange and methylene blue from aqueous solution with finger-citron-residue-based activated carbon. *Industrial & Engineering Chemistry Research*, 52(39):14297-14303, 2013.

[31] Bulgariu, L., Escudero, L. B., Bello, O. S., Iqbal, M., Nisar, J., Adegoke, K. A., and Anastopoulos, I. The utilization of leaf-based adsorbents for dyes removal: A review. *Journal of Molecular Liquids*, 276:728-747, 2019.

[32] Wu, Z., Zhong, H., Yuan, X., Wang, H., Wang, L., Chen, X., and Wu, Y. Adsorptive removal of methylene blue by rhamnolipid-functionalized graphene oxide from wastewater. *Water Research*, 67:330-344, 2014.

[33] Liu, Q., Li, Y., Chen, H., Lu, J., Yu, G., Möslang, M., and Zhou, Y. Superior adsorption capacity of functionalised straw adsorbent for dyes and heavy-metal ions. *Journal of Hazardous Materials*, 382:121040, 2020.